Modified Hecht model qualifying radiation damage in standard and oxygenated silicon detectors from 10 MeV protons

A. Charbonnier [a], S. Charron [a], A. Houdayer [a], C. Lebel [a,1], C. Leroy [a], V. Linhart [b], S. Pospíšil [b]

[a] *Université de Montréal, Montréal (Québec) H3C 3J7, Canada*

[b] *Institute of Experimental and Applied Physics of the CTU in Prague, Horská 3a/22, CZ-12800 Praha 2 - Albertov, Czech Republic*

Abstract

The Hecht model describes the charge collection efficiency of semiconductor detectors using the mean free path of the charge carriers. While the fit to data are accurate for non-irradiated detectors, modifications are necessary to take into account the structural changes in the detectors induced by their exposition to high particle fluences. A modified model will be presented. In this model, the mean free path depends on the shape of the electric field and on the charge carriers lifetimes. The lifetimes were measured experimentally from the front- and back-illumination of the detectors by 660 nm laser light and by alphas from an ^{241}Am source. This new Hecht model was fitted to alpha and beta charge collection efficiencies of standard and oxygenated silicon detectors after their irradiation by 10 MeV protons with fluences varying from 10^{11} to 3×10^{14} p/cm^2.

Introduction

The Hecht model [1] fails to describe the charge collection efficiency (CCE) for particles that stop in non-irradiated detectors and any charge collection in irradiated detectors, including for minimum ionising particles (mips). The new Hecht model proposed here includes a natural variation of the CCE with the decrease of the effective carrier lifetime with increasing particle fluence. It also introduces a small exponential component to the electric field sufficient to greatly improve the description of CCE for exposition of the detectors to particles that stop in the non-depleted region of the detectors. It is also shown that for 10 MeV protons, the presence of oxygen in irradiated standard planar silicon detectors slightly slows down the degradation of electrical characteristics but does not affect the detectors performance. The radiation hardness improvement found is small compared to what has been observed for 24 GeV/c protons [2].

[1] corresponding author, e-mail address: lebel@lps.umontreal.ca

1 Experimental Setups

The detectors used to validate the model are standard planar silicon squared pad detectors from CiS Institute [3] using <111> silicon grown by Wacker Siltronics [4]. Two sets of detectors were irradiated: one with material submitted to oxygen diffusion (SP-oxy) and one with material without oxygen diffusion (SP). The diffusion was performed in nitrogen atmosphere at 1150°C and the oxygen concentration achieved was $\approx 3 \times 10^{17}$at/cm^3. All detectors had a thickness of 280±5 μm and an area of 0.25 cm^2. The initial resistivities were 4.0 kΩ·cm and 4.9 kΩ·cm for the SP-oxy and SP detectors, respectively.

The detectors were irradiated by 10 MeV protons at various fluences with the Tandem accelerator of the University of Montreal. They were irradiated by pairs (SP and SP-oxy) to allow a point by point fluence comparison. Several points were taken at fluences varying from 1×10^{11} p/cm^2 to 3×10^{14} p/cm^2. The irradiation time varied between a few minutes and two hours to insure uniform exposition of the detectors and to avoid annealing as much as possible. The detectors were stored in a cold environment at −20°C after their irradiation. IV-CV measurements were done after an annealing treatment of 4 minutes at 80°C was performed on the detectors [5] (equivalent to about 21 days at room temperature).

The full depletion voltage (V_{fd}) was extracted from the C-V curves and the effective doping concentration (N_{eff}) was calculated using $|N_{eff}| = \frac{2\epsilon V_{fd}}{qw^2}$ where ϵ is the silicon electric permittivity, q is the elementary charge and w is the detector thickness. The N_{eff}, which saturated for high fluences, was fitted to the data (see Fig. 1a) according to

$$|N_{eff}| = |N_{eff,0}\exp(-c\Phi) - N_{sat}(1-\exp(-c_c\Phi))| \quad (1)$$

The initial effective doping concentration $N_{eff,0}$ was $9.6\pm0.3\times10^{11}$/cm^3 for SP and $11.3\pm0.4\times10^{11}$/cm^3 for SP-oxy detectors. The donor removal constant c was $9.5\pm0.8\times10^{-14}$cm^2 and $10.0\pm0.6\times10^{-14}$cm^2 for SP and SP-oxy detectors, respectively. The saturation doping concentration N_{sat} and acceptor creation constant c_c were $43.8\pm7.4\times10^{11}$/cm^3 and $1.4\pm0.3\times10^{-14}$cm^2 for SP and $50.1\pm2.9\times10^{11}$/cm^3 and $0.80\pm0.07\times10^{-14}$cm^2 for SP-oxy detectors, respectively. The fit of Eq. 1 to the data in Fig. 1a clearly shows that the type-inversion fluence is further for SP-oxy than SP detectors indicating a better radiation hardness.

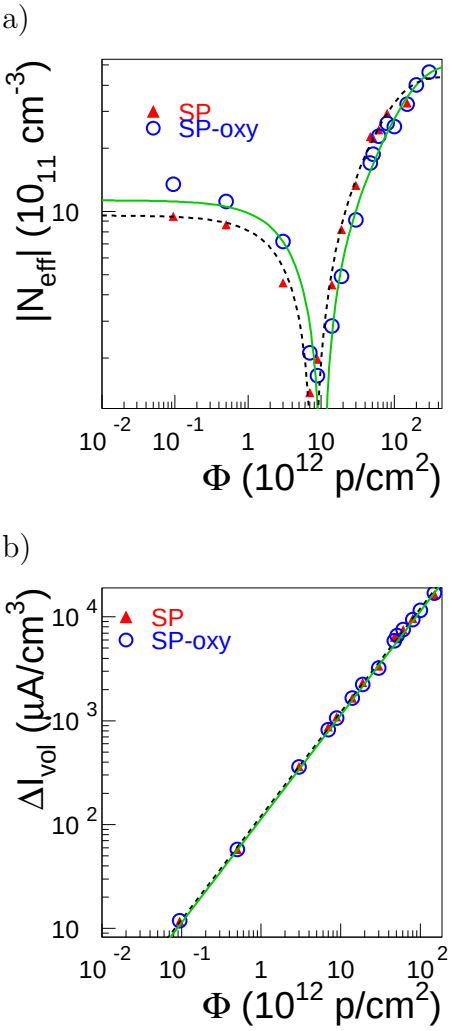

Fig. 1. a) Effective doping concentration and b) leakage current variation with increasing 10 MeV proton fluence for SP and SP-oxy silicon detectors.

As for the volumic leakage current, it increases linearly with fluence ($\Delta I_{vol} = \alpha\Phi$) as can be seen in Fig. 1b. The leakage current of SP detectors increases slightly faster as indicated by the higher radiation-induced reverse current damage constant: α=12.1±0.2×10^{-17} A/cm instead of α=11.4±0.2×10^{-17} A/cm for the SP-oxy detectors. Therefore, oxygen diffusion slows down the degradation of the detectors.

1.1 *Lifetime Measurements*

The carriers lifetimes measurements were done using a 660 nm laser beam and an ^{241}Am source. The lifetimes were extracted using a method described in Ref. [6] which consists of correcting the current as a function of time for trapping effects.

For the laser setup, the beam was impinging on the laser window of the detectors on the front and on the grid electrode on the back. The photons have an average penetration length of about 3 μm. Therefore, it is possible to consider that all the electron-hole pairs are created at the electrode, allowing the study of one carrier at a time. Hence, the holes and electrons can be measured from back and front illumination, respectively. In the second setup, the distance between the ^{241}Am source and the detector was 1.15 cm and the measurement was performed in air. Therefore, the α-particles had an average energy of 4.4 MeV when reaching the detector (range in silicon of about 20 μm). The carriers were still considered as isolated (only one carrier contributes to the total charge).

This method has two drawbacks: it requires that the lifetime is short enough to be measured and that enough measurements are taken beyond V_{fd}. The first requirement forbids the analysis at low fluences. The second requirement excludes very high fluences in which leakage current is so high that full-depletion is barely or not reachable.

The results for electron and hole lifetimes are shown in Fig. 2 for SP (a,c) and SP-oxy (b,d) detectors. The low-fluence lifetimes found from the α-measurements are underestimated since the carriers reach the electrodes with collection times shorter than their lifetimes. Combining laser and α measurements data beyond $\Phi = 3 \times 10^{12}$p/cm^2, Eq. 2 can be fitted to the data and the parameter β, the effective trapping time damage constant, can be extracted [7]:

$$\frac{1}{\tau} = \beta\Phi \qquad (2)$$

The results of the fit are for SP detectors: $\beta_e = 0.878 \pm 0.004 \times 10^{-6}$cm^2/sec and $\beta_h = 1.226 \pm 0.007 \times 10^{-6}$cm^2/sec and for SP-oxy detectors: $\beta_e = 1.075 \pm 0.003 \times 10^{-6}$cm^2/sec and $\beta_h = 0.902 \pm 0.005 \times 10^{-6}$cm^2/sec.

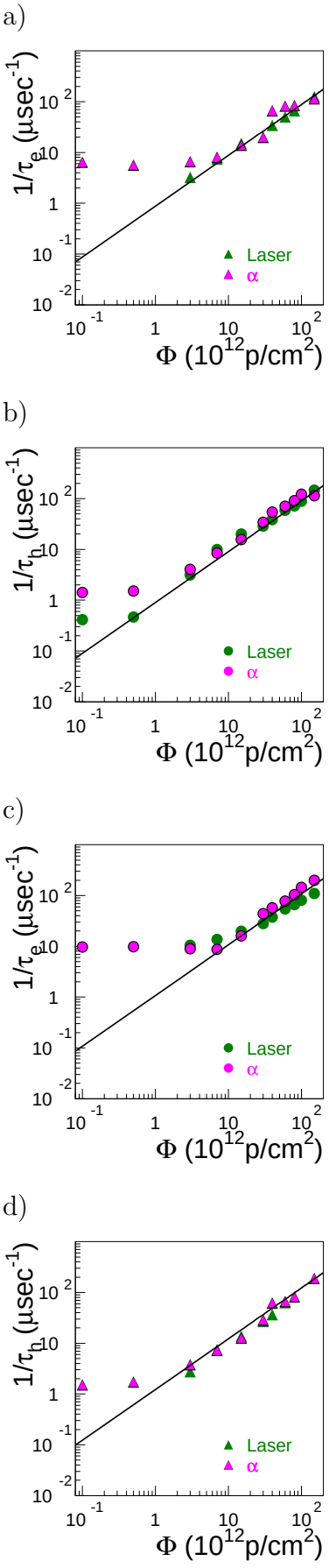

Fig. 2. a,c) Electron and b,d) hole inverse lifetime dependence on proton fluence for SP (a-b) and SP-oxy (c-d) detectors. The line corresponds to the fit of Eq. 2 to the data with $\Phi \geq 3 \times 10^{12}$p/cm^2.

Standard spectroscopic measurements were performed using a multiple α-source in vacuum. The source contained ^{239}Pu, ^{241}Am and ^{243}Cm with main peak energies of 5.15 MeV, 5.49 MeV and 5.80 MeV, respectively. Only the highest peak, the ^{239}Pu peak, was used to determine the CCE for front- and back-side illumination. The spectra were recorded using a charge-sensitive preamplifier, followed by a linear shaping amplifier and finally, a multi-channel analyzer.

A second spectroscopic setup was used to measure the CCE of the detectors when exposed to mips, in the present case β^-. The detectors were positionned in front of a ^{90}Sr-Y source emitting electrons with a maximum energy of 2.28 MeV and average energy of 0.76 MeV. To insure that only mips signal would be recorded, a surface-barrier silicon detector was located at the back of the detector tested. The acceptance window of the trigger detector was delimited to select only the mips. The signal from both detectors went into charge preamplifiers. Then, the output went into acquisition cards which converted the exponential signal from the preamplifiers into histograms. At this step, the coincidence of events was evaluated. The beta spectrum was analysed using a Landau fit to the data.

2 The Hecht Model

When considering the total charge at the electrodes of a planar detector of thickness w, one can find that for a electron-hole pair creation site x_0, the CCE will depend on the mean free path ($\Lambda_{e,h}$) of both carriers (e: electron, h: hole) [8].

$$\begin{aligned}\mathrm{CCE}(x_0) = &\tfrac{\Lambda_e}{w}\left[1-\exp\left(-\tfrac{w-x_0}{\Lambda_e}\right)\right] \\ &+ \tfrac{\Lambda_h}{w}\left[1-\exp\left(-\tfrac{x_0}{\Lambda_h}\right)\right]\end{aligned} \tag{3}$$

The free path of the carriers $\lambda_{e,h}(x)$ can be described in terms of mobility $\mu_{e,h}(x)$, electric field $E(x)$ and carrier lifetime $\tau_{e,h}$.

$$\begin{aligned}&\lambda_{e,h}(x) = \mu_{e,h}(x)E(x)\tau_{e,h} \\ &\text{with} \quad \mu_{e,h}(x) = \tfrac{\mu_0}{[1+(\mu_0 E(x)/v_s)^m]^{1/m}}\end{aligned} \tag{4}$$

where $\mu_0 = 1350\mathrm{cm}^2/\mathrm{Vsec}$, m=2 and the saturation velocity is v_s=1.05×10^{7}cm/sec for electrons and $\mu_0 = 450\mathrm{cm}^2/\mathrm{Vsec}$, m=2 and v_s=1.00×10^{7}cm/sec for holes [8]. All these values are for experiments performed at room temperature. The free path ($\lambda_{e,h}$) is averaged over the path of the carrier between the creation site and the collecting electrode.

$$\begin{aligned}\Lambda_e = \overline{\lambda_e(x)} = \tfrac{1}{w-x_0}\textstyle\int_{x_0}^{w}\mu_e E\tau_e\cdot dx \\ \text{and} \quad \Lambda_h = \overline{\lambda_h(x)} = \tfrac{1}{x_0}\textstyle\int_{0}^{x_0}\mu_h E\tau_h\cdot dx\end{aligned} \tag{5}$$

The Hecht model presented in Eq. 6 uses Eq. 5 in Eq. 3 and renormalizes over all possible pair creation sites depending on the type and energy of the particle entering the detector.

$$\mathrm{CCE} = \frac{1}{w}\int_0^w \mathrm{CCE}(x_0)\cdot f(x_0)dx_0 \tag{6}$$

It can be used for all types of particles at any energy. The energy deposition probability is given by the function $f(x_0)$ in Eq. 6. For β-particles, this function is equal to 1 and for α-particles, it is the energy deposition as described by the Bragg peak renormalized to the total energy of the particle.

Standardly, the electric field in the silicon detectors is considered as an abrupt pn junction. For back illumination, this description implies that the collected charge should be strictly zero if the path of the particle is outside the depleted region ending at x_d. However, it is experimentally observed that there is some charge collected before this depletion region is reached. Therefore, the abrupt junction model is insufficient to account for charge collection for back illumination. The addition of a small exponential component to the electric field reaching the back of the detector provides the extra charge required to characterize the entire CCE curve both from the back- and front-side illumination. The new electric field has the form depicted in Eq. 7.

$$E(x) = \begin{cases} -\frac{qN_a}{\epsilon}(x + x_p) \\ \text{for } [-x_p, 0] \\ \frac{qN_d}{\epsilon}\left(x - x_c - \frac{1}{a} - \frac{x_c - w}{\mathrm{e}^{-a(x_c-w)}}\right) \\ \text{for } [0, x_c] \\ -\frac{qN_d}{\epsilon \mathrm{e}^{-a(x_c-w)}}\left[\frac{1}{a}\left(\mathrm{e}^{-a(x_c-w)} - 1\right) + (x_c - w)\right] \\ \text{for } [x_c, w] \end{cases} \quad (7)$$

where x_p is the width of the p^+-region and N_a the acceptor concentration in the same region while x_c is the position where the change in electric field occurs in the part of the detector with donor concentration N_d. The parameter a in Eq. 7 has to be defined with respect to the potential applied. The position x_c is a parameter very close to the deserted width x_d but slightly closer to the front electrode to keep the same potential in the detector.

This description (Eq.7) of the electric field correspond to non-irradiated detectors. Once a detector is irradiated and received an annealing treatment, for a small region at the front surface, the effective doping concentration in this region corresponds to $N_{eff,0}$ (Eq. 1). It must also be taken into account that beyond the inversion fluence, the n-type detector behaves as a p-type detector. Its depletion region is mostly located at the back but also has a component at the front due to the contact of the n-type region, and the front contact p^+. The detector has a double-junction [9]: p^+n at the front and pn^+ at the back. In Fig. 3, the electric field is shown in the case of irradiated detectors.

3 Modelized Charge Collection Efficiency

The new Hecht model introduces two modifications: 1. the mean free path depends on the electric field and on the carrier lifetime, and 2. the electric field has an extra exponential component in the undepleted region. The CCE fit for the passage of a mip in the detector requires only the first modification to the model (see Fig. 4). The addition of the exponential component to the electric field in the undepleted region has little effect since it is insufficient to counter the coulombian interaction between electrons and holes. The mip deposits little energy locally and the electric field at the pair creation site is necessary to avoid initial recombination. For α-particles, the energy deposition is more important and the amount of carriers created is enough to create a distortion in the electric field which allows the charges to separate and avoid the initial recombination.

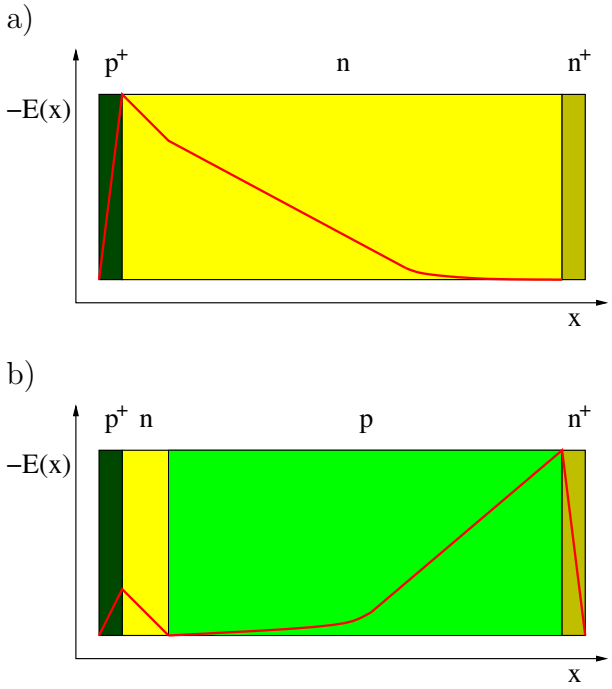

Fig. 3. Electric field description with double-junction for fluences a) before and b) after inversion.

The improvement to the CCE description can mostly be observed for short-range particles. In Figs. 5-6, the full line represents the new model applied to the CCE of SP and SP-oxy detectors only with the introduction of the field-dependent mean free path. It adequately fits all CCE for front-illumination before inversion fluence ($\Phi_{inv} \approx 10^{13}$p/cm^2) and all back-illumination after Φ_{inv}. It is explained by the fact that the depleted region extends from the front before Φ_{inv} (back after Φ_{inv}) and small applied voltages quickly deplete a region greater than the α-particle range. Once all electron-hole pairs are formed in the depleted region, a small modification of the electric field in the non-depleted region is neglectable. For back-illumination for fluences lower than Φ_{inv} and front-illumination for fluences beyond Φ_{inv}, the exponential addition is necessary and allows the model to fit the data appropriately, as shown by the dotted line in Figs. 5-6.

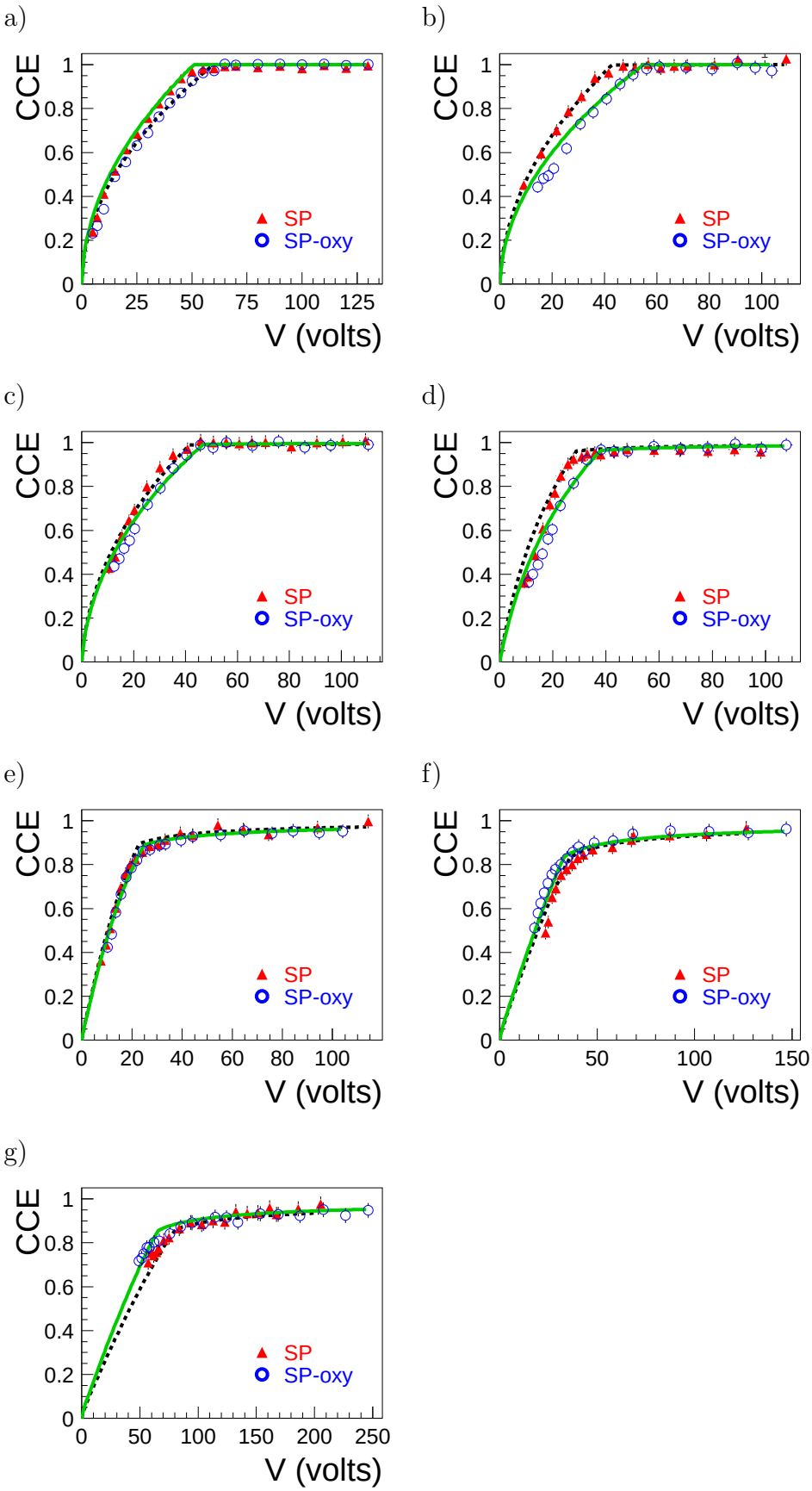

Fig. 4. CCE of SP and SP-oxy detectors exposed to minimum ionizing particles for increasing fluences: a) non-irradiated, b) $\Phi = 1 \times 10^{11}$ p/cm^2, c)$\Phi = 5 \times 10^{11}$ p/cm^2, d)$\Phi = 3 \times 10^{12}$ p/cm^2, e)$\Phi = 7 \times 10^{12}$ p/cm^2, f)$\Phi = 1.5 \times 10^{13}$ p/cm^2, g)$\Phi = 3 \times 10^{13}$ p/cm^2. The dotted and full lines represent the application of the model to SP and SP-oxy detectors, respectively.

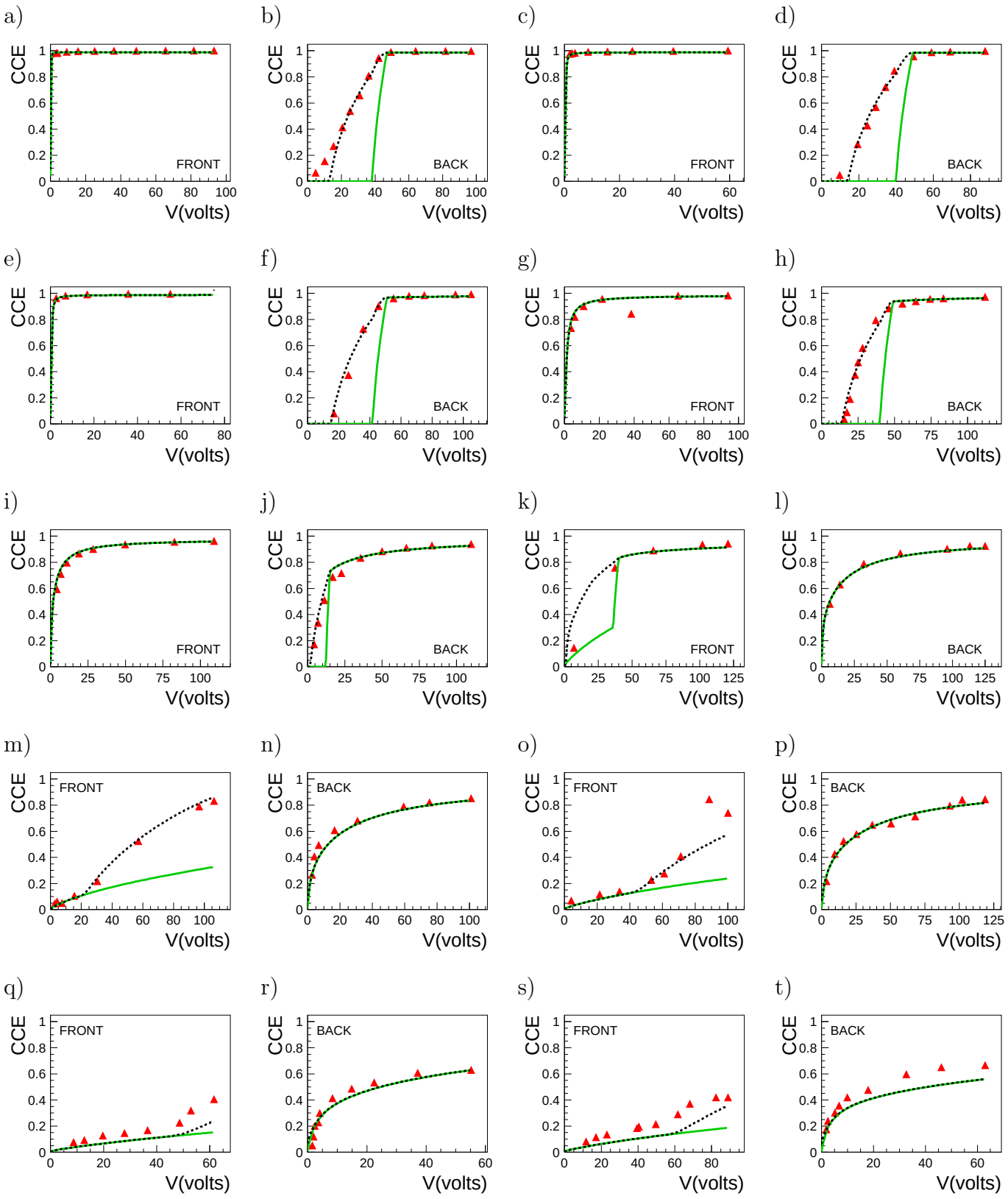

Fig. 5. Charge collection efficiency of SP silicon detectors exposed to α-particles. The lines represent the new Hecht model with (dotted line) and without (full line) exponential component to the electric field. c) and d) $\Phi = 1 \times 10^{11}$p/cm^2, e) and f) $\Phi = 5 \times 10^{11}$p/cm^2, g) and h) $\Phi = 3 \times 10^{12}$p/cm^2, i) and j) $\Phi = 7 \times 10^{12}$p/cm^2, k) and l) $\Phi = 1.5 \times 10^{13}$p/cm^2, m) and n) $\Phi = 3 \times 10^{13}$p/cm^2, o) and p) $\Phi = 4 \times 10^{13}$p/cm^2, q) and r) $\Phi = 6 \times 10^{13}$p/cm^2 and s) and t) $\Phi = 8 \times 10^{13}$p/cm^2.

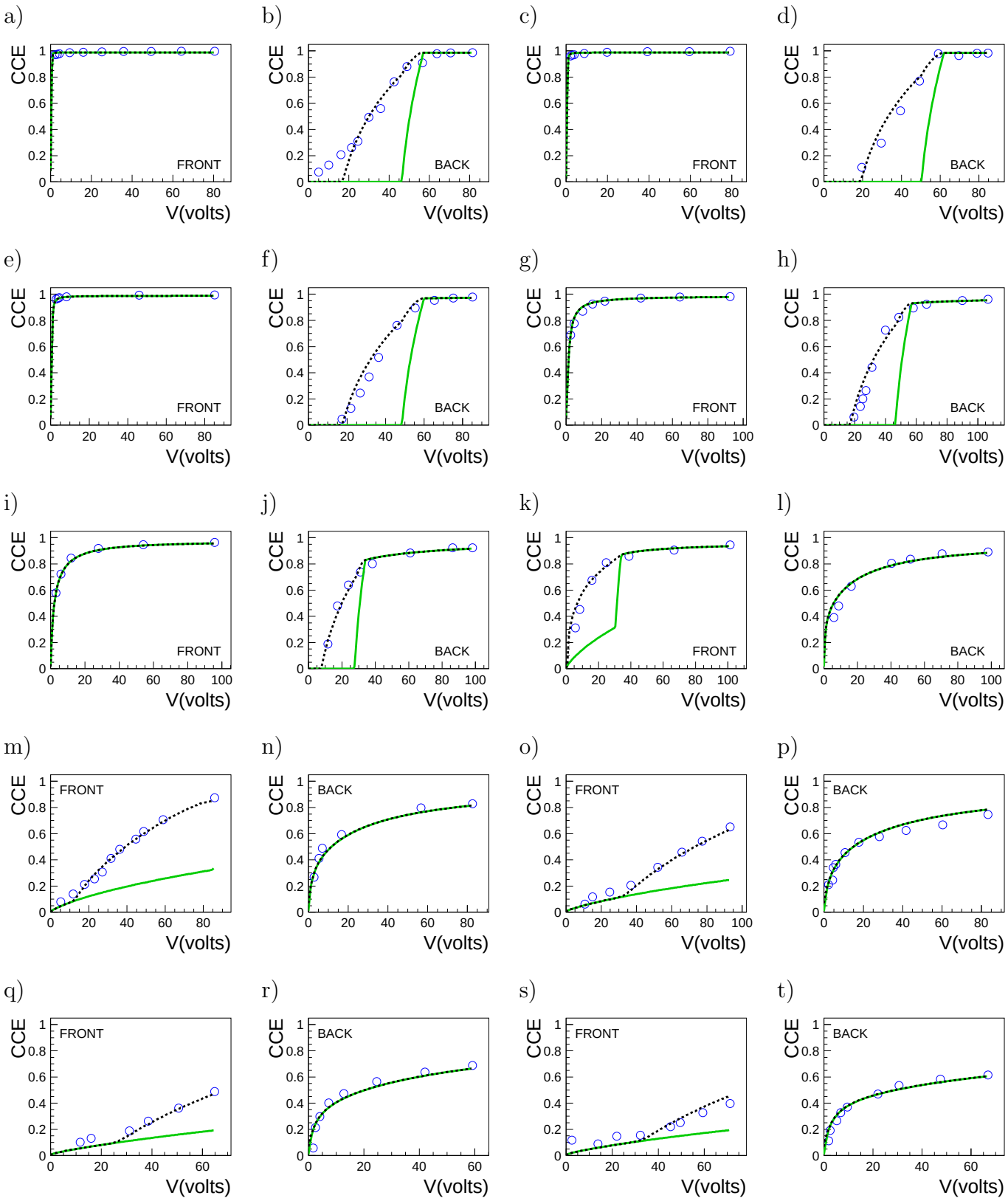

Fig. 6. Charge collection efficiency of SP-oxy silicon detectors exposed to α-particles. The lines represent the new Hecht model with (dotted line) and without (full line) exponential component to the electric field. c) and d) $\Phi = 1 \times 10^{11}$p/cm^2, e) and f) $\Phi = 5 \times 10^{11}$p/cm^2, g) and h) $\Phi = 3 \times 10^{12}$p/cm^2, i) and j) $\Phi = 7 \times 10^{12}$p/cm^2, k) and l) $\Phi = 1.5 \times 10^{13}$p/cm^2, m) and n) $\Phi = 3 \times 10^{13}$p/cm^2, o) and p) $\Phi = 4 \times 10^{13}$p/cm^2, q) and r) $\Phi = 6 \times 10^{13}$p/cm^2 and s) and t) $\Phi = 8 \times 10^{13}$p/cm^2.

The CCE as a function of 10 MeV protons fluence for SP and SP-oxy detectors is presented in Fig. 7. It can be observed that the presence of oxygen does not affect it and that the CCE drops to 80 % at fluences of 8×10^{13}p/cm^2.

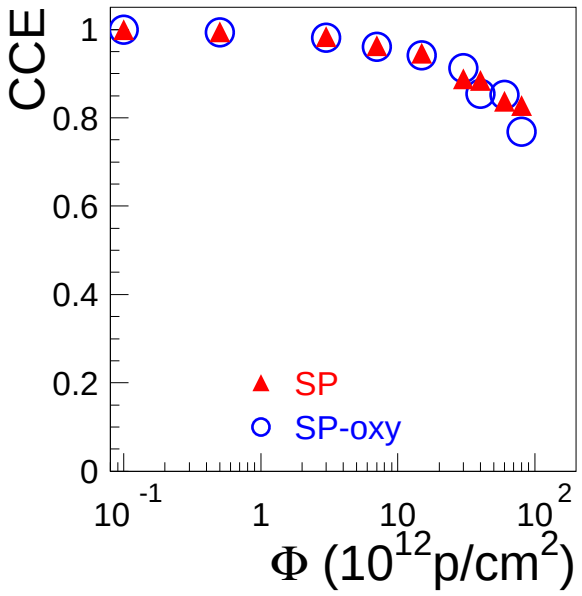

Fig. 7. CCE as a function of fluence of 10 MeV protons for SP and SP-oxy silicon detectors.

Conclusion

The dependence of the mean free path on the electric field and carrier lifetime greatly improves the Hecht model description of the CCE in silicon detectors. When combined with the addition of a small component to the electric field in the non-depleted region, the new model can adequately depict the CCE both for mips and particles that stop in the detector such as α-particles. This model was applied to SP and SP-oxy silicon detectors irradiated with 10 MeV protons. The CCE of both types of detectors was very similar. As for leakage current and effective doping concentration, oxygen diffusion slightly improves the detectors radiation hardness when exposed to 10 MeV protons (Fig. 1) but not as much as it was demonstrated for 24 GeV/c protons [2].

Acknowledgements

This work is financially supported by the Natural Science and Engineering Research Council of Canada (NSERC), by the Fonds Québécois de la Recherche sur la Nature et les Technologies (FQRNT) and by the Czech Ministry of Education, Youth and Sports in frame of the long term research program MSM 6840770029. We would like to thank M. Moll for providing the detectors and for all his help for the measurements performed at CERN.

References

[1] K. Hecht, Z. Phys. 77 (1932) pp. 235-245

[2] G. Lindström et al., (The RD48 (ROSE) Collaboration), *Radiation Hard Silicon Detectors - Developments by the RD48 (ROSE) Collaboration*, Nucl. Instr. and Meth. A 466 (2001) pp.308-326.

[3] CiS Institute für Mikrosensorik, Haabergstrasse 61, 99097 Erfurt, Germany

[4] Wacker Siltronics, Burghausen, Germany

[5] M. Moll, *Radiation Damage in Silicon Particle Detectors - microscopic defects and macroscopic properties* -, Ph.D. thesis, University of Hamburg, December 1999, DESY-THESIS-1999-040, ISSN 1435-8085.

[6] T.J. Brodbeck et al, Nucl. Instr. and Meth. A455 (2000) pp. 645-655

[7] G. Kramberger et al., Nucl. Instr. and Meth. A476 (2002) pp. 645-651

[8] C. Leroy and P.G. Rancoita, *Principle of radiation interaction in matter and detection*, World Scientific Publishing, (2004) 716 pages, and references therein

[9] G. Lutz, Nucl. Instr. and Meth. B95 (1995) pp. 41-49; C. Leroy et al., Nucl. Instr. and Meth. A434 (1999) pp. 90-102